Structural Relaxation of Polymer Nanospheres under Soft and Hard Confinement: Isobaric *versus* Isochoric Conditions

Yunlong Guo,[†] Chuan Zhang,[†] Christine Lai,[†] Rodney D. Priestley,[†,*] Maria D'Acunzi,[‡] and George Fytas[‡,§]

[†]Department of Chemical and Biological Engineering, Princeton University, Princeton, New Jersey 08544, United States, [‡]Max Planck Institut für Polymerforschung, Ackermannweg 10, 55128 Mainz, Germany, and [§]Department of Materials Science, University of Crete and F.O.R.T.H., Heraklion, Greece

ABSTRACT We have measured the glassy-state structural relaxation of aqueous suspended polystyrene (PS) nanoparticles (the case of soft confinement) and the corresponding silica-capped PS nanoparticles (the case of hard confinement) *via* differential scanning calorimetry. Suspended and capped PS nanoparticles undergo physical aging under isobaric and isochoric conditions, respectively. With decreasing diameter, suspended and capped PS nanoparticles exhibited reduced and bulk glass transition temperatures (T_g), respectively. To account for T_g changes with confinement, all physical aging measurements were performed at a constant value of $T_g - T_a$, where T_a is the aging temperature. With decreasing diameter, aqueous suspended PS nanoparticles exhibited enhanced physical aging rates in comparison to bulk PS. Due to differences in thermodynamic conditions during aging and interfacial effects from nanoconfinement, at all values of $T_g - T_a$ investigated, capped PS nanoparticles aged at reduced rates compared to the corresponding aqueous suspended PS nanoparticles. We captured the physical aging behavior of all nanoparticles *via* the Tool, Narayanaswamy, and Moynihan model of structural relaxation.

KEYWORDS: structural relaxation · confinement · nanoparticles · core–shell nanoparticles · glass transition · physical aging · TNM model

Understanding the dynamics of nanoscopically confined polymer remains an intriguing scientific endeavor and one with significant technical motivation. Confined polymers are featured prominently in emerging applications ranging from nanostructured films for plastic solar cells to polymer nanocomposites for structural applications, and to thin films for smart coatings, photoresists for patterning of submicrometer features, and membranes for energy-efficient separations.[1−5] When a polymer film (freestanding or substrate-supported) is confined to the nanoscale, its glass transition temperature (T_g) and associated dynamics can differ substantially from the bulk.[6−19] Factors that influence the deviation in T_g with confinement include geometry,[20] strength of interfacial interactions,[14,21] sample preparation,[22] and chemical structure.[23]

The importance of confined polymers for nanotechnology, as well as scientific curiosity, has motivated experimental studies to characterize and elucidate the cause of the T_g confinement effect. Numerous reviews[9,15,24] highlighting the experimental and computational studies have been written. The initial work by Keddie *et al.*[11] demonstrated the dependence of polymer–substrate interactions on the deviation in T_g with confinement of thin films, which has been subsequently confirmed by others.[10,25,26] In essence, in the absence of strong polymer–substrate interactions, decreases in T_g with confinement presumably occur due to free surface effects.[6,8] This assertion was supported by measurements of freestanding films (two free surfaces) in which the magnitude in T_g reduction due to confinement was significantly greater than that of supported films (one free surface) with similar thickness[9] and direct measurements of a reduced free surface layer T_g of single substrate support films.[8,17,27] However, we note that the impact of confinement on T_g is still a subject of much debate.[28−33]

Irrespective of deviations in T_g with confinement, confined glasses undergo structural relaxation (*i.e.*, physical aging). Structural relaxation is the spontaneous relaxation of glasses toward equilibrium, which results in a time dependence of end use properties. Aside from investigations on submicrometer thick polymeric membranes,[34,35] few studies have characterized the structural relaxation of confined polymer glasses.[17,36−43] Reductions in the rate-of-aging were reported for supported thin polymer films of poly(methyl methacrylate) (PMMA)[38] and poly(2-vinyl pyridine) (P2VP),[41] and polymer–silica nanocomposites of PMMA and P2VP[39,41,44]

* Address correspondence to rpriestl@princeton.edu.

Received for review December 21, 2010 and accepted June 24, 2011.

Published online June 30, 2011
10.1021/nn201751m

compared to the corresponding bulk polymer. Suppressed aging with confinement has been attributed to interfacial effects perturbing glassy-state dynamics.[38,39,41] This assertion was supported by local interfacial aging measurements of PMMA films supported on silica that revealed a nearly complete suppression of aging within the first 25 nm of the interface.[17] Recently, simulations also support the idea that strongly impeded glassy-state dynamics at the polymer−substrate interface can lead to suppressed aging of confined polymer.[45,46] In the absence of interfacial effects, the rate-of-aging of ultrathin polystyrene films has been reported to be comparable to or enhanced relative to that of the bulk.[37,38,40]

Since glasses are non-equilibrium materials, their properties depend on the path to formation.[47] Different thermal histories (*e.g.*, cooling rate), environmental conditions (*e.g.*, humidity), and pressure during formation lead to glasses with different thermodynamic properties. Given that their properties strongly depend on the path to formation, it is easy to comprehend the challenge of understanding confinement effects on aging of glasses. Here, we advance the current understanding of how confinement impacts aging by investigating how different confinement conditions, such as soft *versus* hard confinements, alter the rate of structural relaxation and the time required to reach equilibrium. This is achieved *via* aging studies on aqueous suspended polystyrene (PS) nanoparticles (the case of *soft* confinement) and silica-capped PS core−shell nanoparticles (the case of *hard* confinement) by calorimetry. For aqueous suspended PS nanoparticles, structural relaxation is under isobaric conditions, while for silica-capped PS nanoparticles, structural relaxation is under isochoric conditions. We show that the type of confinement has a significant effect on the deviation in structural relaxation of confined glasses compared to the bulk.

RESULTS

Figure 1 illustrates the temperature protocol employed for the aging test, which consisted of four major steps: (A) sample equilibration (annealing at $T_g + 20$ °C for 20 min), (B) measurement of T_g prior to aging experiment, (C) aging or annealing step, and (D) measurement of T_g after aging. The controlled heating rates (in steps B, C, and D) were 20 and 5 °C/min (a lower heating rate is required for the MDSC technique) for the silica-capped PS and aqueous suspended PS nanoparticles, respectively. The cooling rates were 40 °C/min in all experiments. For MDSC measurements, the amplitude was 0.2 °C and the frequency was 0.05 Hz. Reported T_gs are midpoint values.

Figure 2 shows SEM images of 400 nm diameter PS nanoparticles and the corresponding silica-capped PS nanoparticles with a shell thickness of approximately 30 nm before and after the thermal protocol

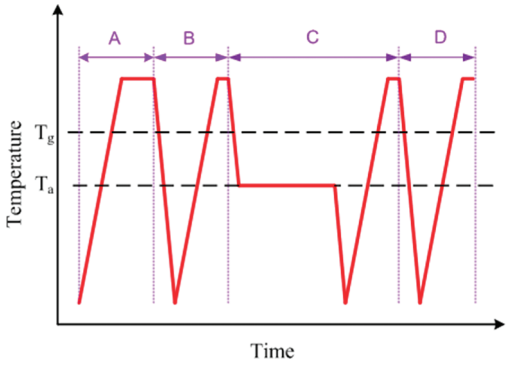

Figure 1. Temperature protocol of aging test: (A) removal of previous thermal history, (B) measurement of T_g prior to aging step, (C) aging step, and (D) measurement of T_g after aging step.

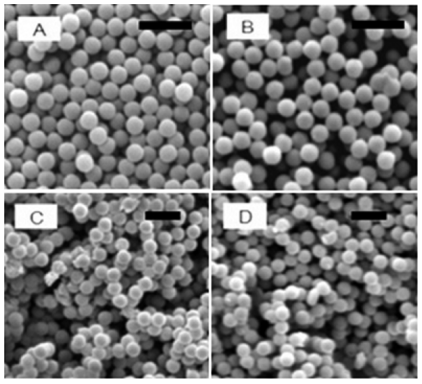

Figure 2. SEM images of 400 nm diameter PS nanoparticles and the corresponding silica-capped PS nanoparticles before and after aging (scale bars = 1 μm): (A) PS nanoparticles before aging, (B) PS nanoparticles after aging, (C) silica-capped PS nanoparticles before aging, and (D) silica-capped PS nanoparticles after aging.

employed to measure physical aging. Similar SEM images were obtained for 200 nm diameter PS/PS−silica core−shell nanoparticles (shell thickness of ~30 nm). As shown from the representative SEM images, monodisperse, smooth PS nanoparticles were prepared by emulsion polymerization. Coating PS nanoparticles with a thin silica shell *via* the Stöber method did not distort or alter the structure of the nanoparticles, as smooth, monodisperse silica-capped PS nanoparticles were imaged. More importantly, the images show that the nanoparticles were neither destroyed nor did aggregation take place during the thermal protocols employed for aging measurements.

Glass Transition Temperature. Glass transition temperatures were determined during segments B and D of the aging protocol. Identical T_g values were determined for both segments for all nanoparticle samples, which indicated no coalescence of polymer nanoparticles during the aging protocol, in agreement with SEM images. For bulk PS, $T_{g,bulk}$ = 384 K. Examination of unaged scans for PS nanoparticles (see Figure 3) revealed that soft confinement of PS (nanoparticles

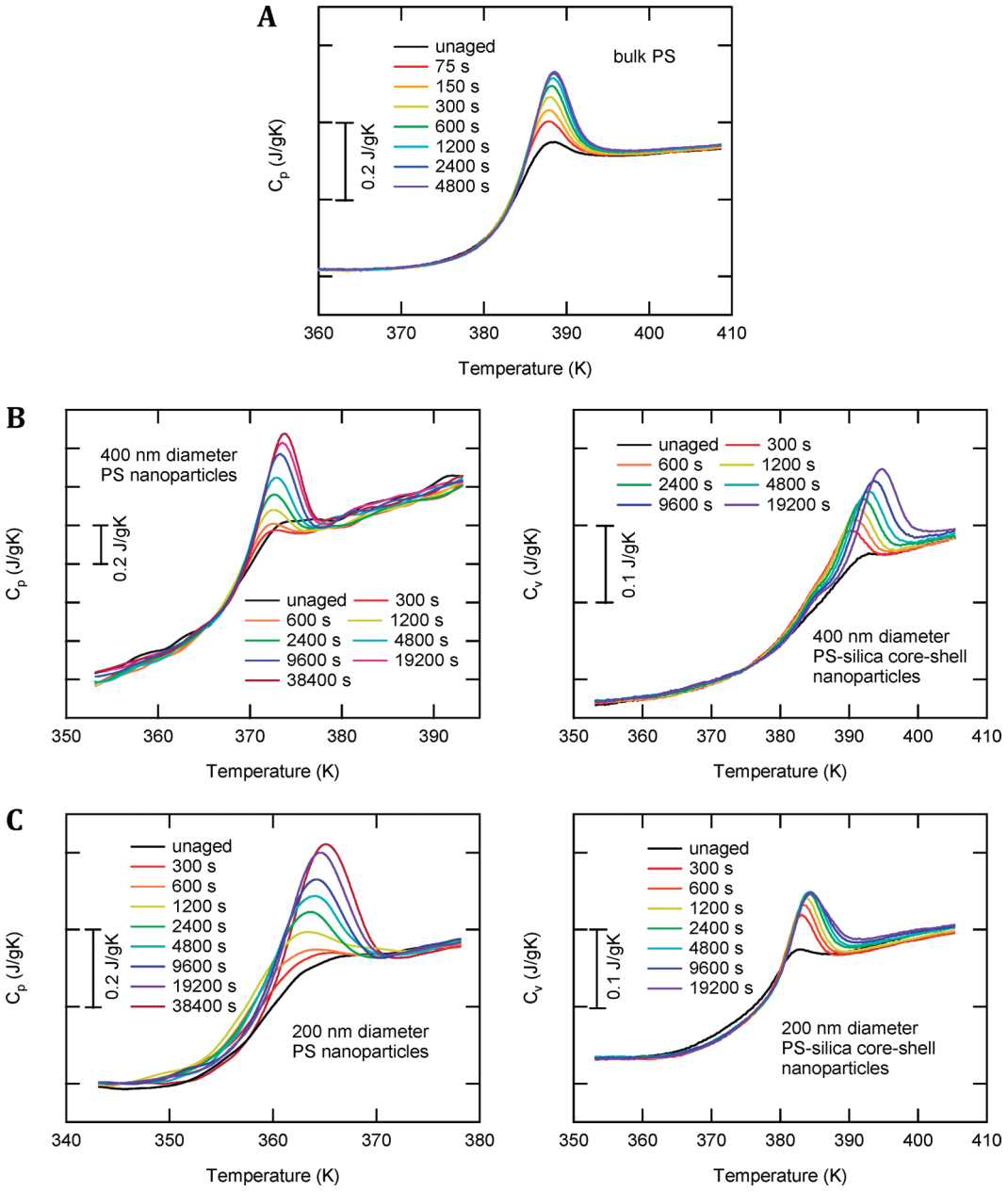

Figure 3. Heat capacity *versus* temperature during aging at $T_g - T_a = 8$ K for (A) bulk PS, (B) 400 nm diameter PS nanoparticles and PS–silica core–shell nanoparticles, and (C) 200 nm diameter PS nanoparticles and PS–silica core–shell nanoparticles.

without silica shell) led to a T_g reduction ($T_{g,d=400\ nm}$ = 370 K; $T_{g,d=200\ nm}$ = 357 K), while hard confinement (nanoparticles with silica shell) resulted in nearly no change in T_g ($T_{g,d=400\ nm}$ = 383 K; $T_{g,d=200\ nm}$ = 378 K). These measurements are consistent with T_g confinement effects previously reported for PS nanoparticles[48] and PS films in the freestanding[10,19] and capped geometries and support the assertion that surface effects play a significant role in altering the T_g of confined polymer.[6,8,13] To account for confinement-induced changes in T_g, aging was compared at a constant value of $T_g - T_a$ for all systems, where T_a was the aging or annealing temperature.

Physical Aging. Figure 3 shows enthalpy recovery curves at $T_g - T_a = 8$ K for different aging times for bulk PS, aqueous suspended PS nanoparticles, and silica-capped PS nanoparticles. During aging, enthalpy recovery curves grew and shifted to slightly higher temperatures until equilibrium was achieved. After an aging time of approximately 40 min (2400 s), equilibrium was achieved for bulk PS. In comparison, PS nanoparticles confined with and without a silica shell continuously exhibited aging at times greater than $t = 320$ min (19 200 s), suggesting a longer aging time to reach equilibrium for both soft and hard three-dimensional confinement.

This observation was further probed by plotting $T_f - T_a$ as a function of aging time at different values of

T_a for bulk PS and PS nanoparticles. The quantity $T_f - T_a$ is a measure of the departure from equilibrium and by definition equals zero at equilibrium; T_f, the fictive temperature, is a measure of the glass structure.[49] The fictive temperature was determined from DSC heat capacity data using a method developed by Moynihan[50] in which T_f is defined as

$$\int_{T_f}^{T_2} (C_{pl} - C_{pg})dT = \int_{T_1}^{T_2} (C_p - C_{pg})dT \qquad (1)$$

where T_1 is a temperature well below T_g at which the measured heat capacity, C_p, and the glassy-state heat capacity, C_{pg}, are the same and T_2 is a temperature well above T_g at which C_p is equal to the liquid heat capacity, C_{pl}. Practically, T_f was determined by setting the area $(T_2 - T_f)(C_{pl} - C_{pg})$ equal to the integral of $(C_p - C_{pg})$ within the temperature interval $[T_1, T_2]$. Figure 4 illustrates aging isotherms for bulk PS and aqueous suspended PS nanoparticles. All aging isotherms asymptotically approached $T_f - T_a = 0$, which indicated the attainment of (or approach to) equilibrium. For all systems, increasing the quench depth $(T_g - T_a)$ resulted in longer aging times required to reach equilibrium. At the same value of $T_g - T_a$, the time required to reach equilibrium, t_{eq}, was significantly shorter for bulk PS than aqueous suspended PS nanoparticles.

Figure 5 shows aging isotherms of PS nanoparticles confined within a silica shell. Similar to bulk and aqueous suspended PS nanoparticles, all aging isotherms asymptotically relaxed to or toward a value of $T_f - T_a = 0$. At the same value of $T_g - T_a$, t_{eq} was shorter for PS nanoparticles confined within a silica shell than aqueous suspended PS nanoparticles. Then it follows that $t_{eq,soft\ confinement} > t_{eq,hard\ confinement} > t_{eq,bulk}$. Yet, we observe that t_{eq} is nearly identical for different sizes of aqueous suspended and silica-capped PS nanoparticles. For the silica-capped PS nanoparticles, this implies that PS and silica do not possess strong attractive interactions, a premise consistent with direct interfacial glass transition temperature measurements of PS supported on a silica substrate.[8] In Figure 5, the solid set of symbols are aging measurements performed at $T_g - 6$ K using MDSC. The data points are consistent with those determined by DSC (open symbols). Hence, the mode of DSC employed should not affect the observed aging isotherms.

We computed aging rates ($R = d(T_f - T_a)/d \log t_{aging}$; with time in seconds) by fitting the linear portion of the aging isotherms to a straight line; the results are summarized in Table 1. Over the aging temperatures probed, bulk PS and 400 nm diameter aqueous suspended PS nanoparticles exhibited similar aging rates. In contrast, 200 nm diameter aqueous suspended PS nanoparticles exhibited aging rates greater than bulk PS. All things being equal, silica-capped PS nanoparticles underwent aging at reduced rates compared to the analogous

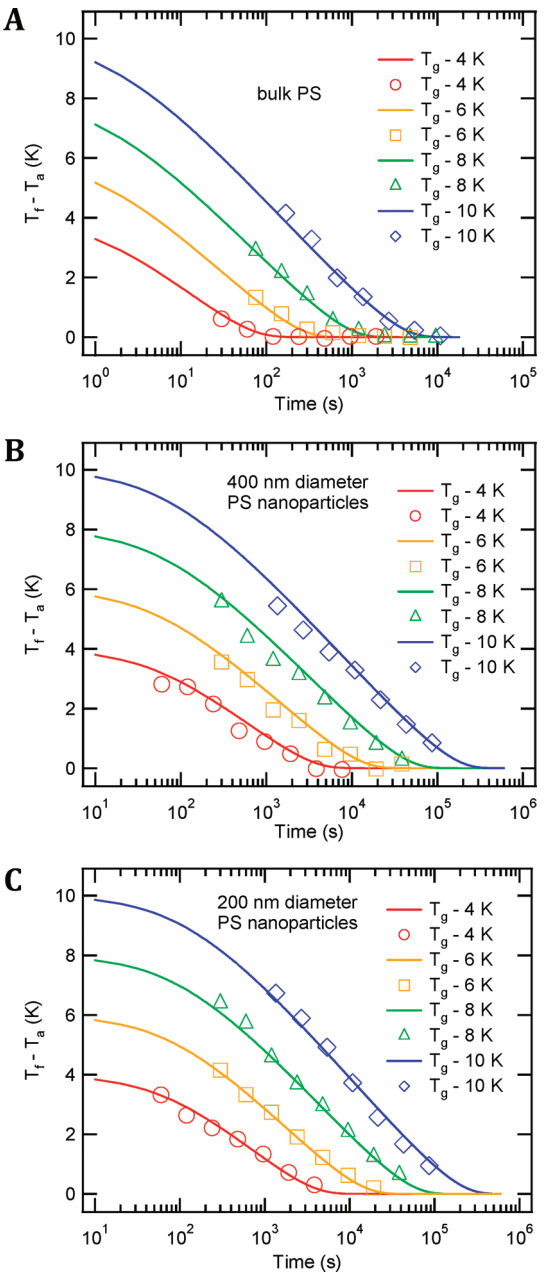

Figure 4. Aging isotherms of (A) bulk PS, and (B) 400 nm diameter and (C) 200 nm diameter aqueous suspended PS nanoparticles aged at different quench depths ($T_g - T_a$). Solid lines are fits to the TNM model (see text). Error bars are smaller than symbol sizes and were determined as the standard deviation from multiple tests.

aqueous suspended PS nanoparticles. The percentage reduction in aging rate (averaged over all aging temperatures investigated) was similar for both 400 and 200 nm PS nanoparticles with the addition of a silica shell.

Modeling Physical Aging of Polymer Nanoparticles. Aging, a nonlinear and non-exponential relaxation process in which enthalpy manifests time-dependent behavior, is often described by the Tool, Narayanaswamy, and Moynihan (TNM) model[51−53] and the Kovacs, Aklonis, Hutchinson, and Ramos (KAHR) model,[54] which are

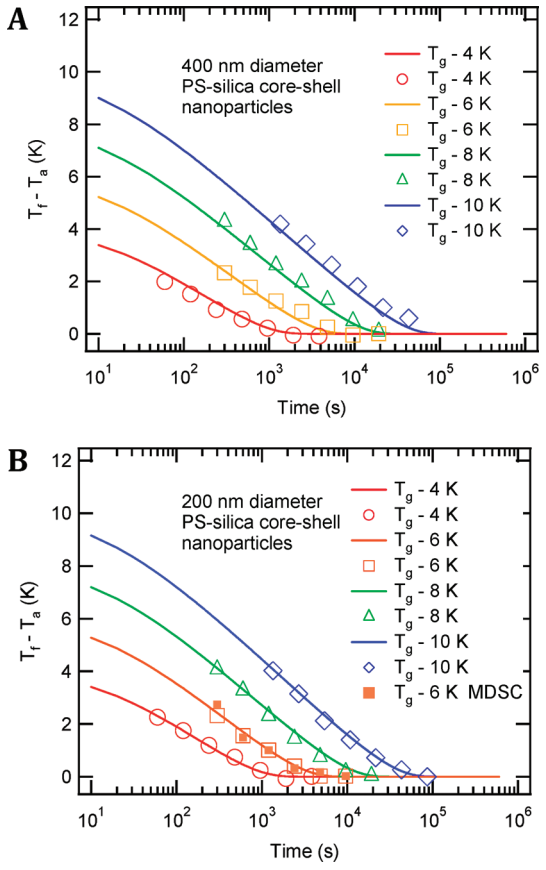

Figure 5. Aging isotherms of (A) 400 nm diameter and (B) 200 nm diameter PS–silica core–shell nanoparticles aged at different quench depths ($T_g - T_a$). Solid lines are fits to the TNM model (see text). Filled squares are data measured by MDSC. Error bars are smaller than symbol sizes and were determined as the standard deviation from multiple tests.

TABLE 1. Aging Rates (*R*, unit: K) of Bulk and PS Nanoparticles at Different Aging Temperatures[a]

	temperature (K)			
size and structure	$T_g - 4$	$T_g - 6$	$T_g - 8$	$T_g - 10$
d = 200 nm				
core	1.996	2.491	2.824	3.077
core–shell	1.885	2.371	2.662	2.878
d = 400 nm				
core	1.912	2.383	2.739	2.972
core–shell	1.818	2.302	2.573	2.786
bulk PS	1.679	2.312	2.699	2.895

[a] The error in aging rates is about ±0.074 and was determined as the average standard deviation in aging rates from multiple tests.

mathematically equivalent. The TNM model utilizes the Kohlrausch–Williams–Watts (KWW)[55] function to represent structural relaxation during aging, and for enthalpy relaxation is given by

$$\delta_h = \Delta H_{a,\infty} - \Delta H_a(t) = \delta_{h0}\exp\left[-\left(\int_0^t \frac{dt}{\tau}\right)^{\beta}\right] \quad (2)$$

TABLE 2. TNM Model Parameters of $\Delta h/R$, x, and β for Fitting of Bulk PS and PS Nanoparticles

		400 nm		200 nm	
	bulk PS	400 nm PS	PS–silica	200 nm PS	PS–silica
$\Delta h/R$ (K)	83400	81300	83700	78700	83000
ln A (s)	−212.49	−215.04	−215.17	−215.75	−214.91
x	0.18	0.19	0.07	0.27	0.13
β	0.43	0.84	0.83	0.86	0.89

where δ_h, the departure from equilibrium, is defined as the difference between the equilibrium enthalpy loss ($\Delta H_{a,\infty}$) and the instantaneous enthalpy loss of the glass (ΔH_a), as such, δ_{h0} is the initial enthalpy departure from equilibrium. The parameter τ is the characteristic relaxation time, and β is the non-exponential parameter related to the width of the relaxation time distribution. The relaxation time, which is dependent on temperature and structure, is approximated by

$$\ln \tau = \ln A + \frac{x\Delta h}{RT} + \frac{(1-x)\Delta h}{RT_f} \quad (3)$$

where the parameter A is a material constant, x partitions the structure and temperature dependence on τ, and $\Delta h/R$ is the relative activation energy. The relationship between T_f and δ_h is given by

$$T_f = T_a + \frac{\delta_h}{\Delta C_p} \quad (4)$$

where ΔC_p is the change in heat capacity at T_g. When eqs 2–4 (TNM model) are applied, aging can be modeled by calculating the evolution of the fictive temperature as a function of time.[56]

The relative activation energies ($\Delta h/R$) were determined experimentally for each sample as the slope from Arrhenius plots of ln(cooling rate) *versus* ($1/T_f$).[37] The parameters A, x, and β were identified by best fits to the experimental data (see Table 2) *via* minimizing the sum of χ^2 error between the desired fitting functions and the data. The Levenberg–Marquardt algorithm was used to search the parameter space for the minimum of χ^2.[57] The initial value of A was set according to $\ln A = \ln \tau_{T_g} - \Delta h/RT_g$, with τ_{T_g} = 100 s; values of A determined by the fitting are comparable to those found in the literature.[58]

Solid lines in Figure 4 are fits to the TNM model using eqs 2–4. The model provided a good fit to the experimental data for bulk PS and aqueous suspended PS nanoparticles. Activation energies for aqueous suspended PS nanoparticles were slightly lower than bulk PS. The partition parameter, x, and stretched exponential parameter, β, were larger with soft confinement when compared to bulk PS at identical values of $T_g - T_a$. At early aging time, the initial plateau was predicted to be longer for aqueous suspended PS nanoparticles compared to bulk PS.

Capping of the PS nanoparticles with a thin silica shell, *via* the Stöber method, was accomplished at ~296 K

(room temperature). Therefore, at room temperature, the nanoparticles should be considered in a stress-free state, and the pressure within the core–shell nanoparticle should be atmospheric. If the silica shell was rigid and free of cracks, then upon heating, due to differences in thermal expansion coefficients between PS and silica, glass formation and aging would be under nearly isochoric conditions. Additionally, a positive pressure would develop within the core–shell nanoparticles. The condition of constant volume was confirmed by comparing the constant pressure heat capacity, C_p, for the aqueous suspended PS nanoparticles to the constant volume heat capacity, C_v, of the silica-capped PS nanoparticles at T_g to the thermodynamic relationship

$$C_p - C_v = \frac{T\alpha^2}{\rho\kappa} \quad (5)$$

where α is the coefficient of thermal expansion, κ is the compressibility, and ρ is the density. Table 3 lists the change in heat capacity at T_g for bulk and PS nanoparticles. The differences in heat capacity between aqueous suspended and silica-capped PS nanoparticles are consistent with eq 5.

The expression between the T_f and δ_h (see eq 4) was modified to account for the isochoric relaxation of silica-capped PS nanoparticles

$$T_{f,\text{core-shell}} = T_a + \frac{\delta_h}{\Delta C_v} \quad (6)$$

The solid lines in Figure 5 are fits to the data using the TNM model, eqs 2, 3, and 6. The model provided a good description of the experimental data. Silica-capped PS nanoparticles exhibited higher and lower values of activation energies and x, respectively, compared to aqueous suspended PS nanoparticles. Values of β remained nearly unchanged for PS nanoparticles with and without a silica shell.

DISCUSSION

This work presents a comparison of soft and hard confinement effects on physical aging of polymer glasses. Studies on polymer nanoparticles with and without an outer inorganic shell allow for independent studies of confinement and interfacial effects on aging. When investigating the impact of confinement on physical aging, the importance of maintaining a constant quench depth is due to the strong nonlinear dependence of aging rate on the aging temperature.[59] The temperature dependence of the physical aging rate is set by the synergism between the driving force for aging ($T_g - T_a$) and the mobility (T_a). Yet, two assumptions must still be made: (1) the temperature dependence of the aging rate is unaffected by confinement, and (2) a constant value of $T_g - T_a$ for bulk and confined polymer necessarily implies equal departures from equilibrium. Regarding the first assumption, for PMMA and PS films supported on silica, the temperature

TABLE 3. Change of Heat Capacity at the Glass Transition for Bulk PS and PS Nanoparticles

			200 nm		400 nm
	bulk	200 nm PS	PS–silica	400 nm PS	PS–silica
ΔC_p, ΔC_v (J/g·K)	0.304	0.311	0.247	0.334	0.266

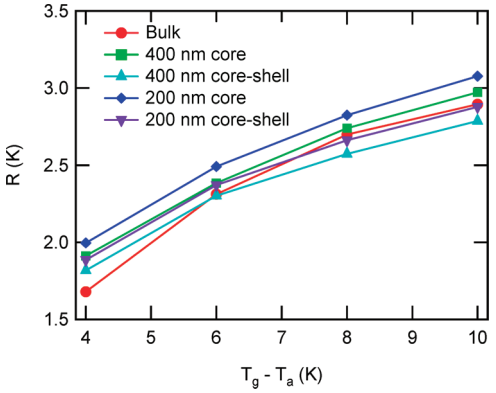

Figure 6. Aging rates of aqueous suspended PS nanoparticles, PS–silica core–shell nanoparticles, and bulk PS at different quench depths ($T_g - T_a$).

dependence of the aging rate (physical aging rate *vs* temperature) was determined to be qualitatively different and similar to the bulk, respectively.[37,38] Additionally, for PMMA, the maximum aging rate occurred at ~300 K for bulk and ~380 K for a 20 nm thick film,[38] while for PS, the maximum aging rate occurred at ~340 K for bulk and ~350 K for a 30 nm thick film.[38] From our analysis of aqueous suspended and silica-capped PS nanoparticles, the temperature dependence of the aging rate was qualitatively similar to that of bulk PS (see Figure 6) and in agreement with the observation reported in refs 37, 38, and 40. We note that in Figure 6, a maximum in aging rate was not observed due to the limited range of aging temperatures probed below T_g. Therefore, we can conclude a similar temperature-dependent aging rate (within the temperature range investigated) for bulk and nanoparticles of PS. Regarding the second assumption, we gain insight into its validity by comparing the actual experimental $T_g - T_a$ (measure of initial departure from equilibrium) values to $T_f - T_a$ values predicted by the TNM model in the early time of structural relaxation for bulk and nanoparticles of PS. For bulk, suspended, and capped PS nanoparticles, the predicted values of $T_f - T_a$ were in agreement with the actual experimental values of $T_g - T_a$ (=4, 6, 8, and 10 K), suggesting an equal departure from equilibrium at the onset of aging.

The work of Koh and Simon, who used DSC to measure structural relaxation of stacked ultrathin PS films at constant quench depths ($T_g - T_a$), provides the best comparison to the present study.[37] They found the time required to reach equilibrium was greater for a thin film (h = 62 nm) compared to bulk and that the logarithmic physical aging rate was independent of film thickness.

Our findings on aqueous suspended PS nanoparticles were reasonably consistent with those of Koh and Simon. As illustrated in Figure 7, longer aging times were required for the attainment of equilibrium for aqueous suspended and silica-capped PS nanoparticles compared to bulk PS. In addition, as shown in Figure 6, we observed similar logarithmic aging rates for bulk and silica-capped PS nanoparticles, while aqueous suspended nanoparticles exhibited slightly higher aging rates. A more direct comparison of confinement effects on aging between polymer nanoparticles and *freestanding* films can be made by defining a characteristic length, h^*, which for nanoparticles was the volume to surface area ratio equal to 1/6 of the diameter, whereas for films, it was taken to be the thickness. For the 400 nm diameter PS nanoparticles, $h^* \sim 67$ nm, while for the 200 nm diameter PS nanoparticles, $h^* \sim 33$ nm. Using this analysis, we found our results to be in good agreement with that of Koh and Simon, that is, an absence of an aging confinement effect on the aging rate for a thin film with $h = 62$ nm and nanoparticles with $h^* \sim 67$ nm. The slight enhancement in aging rate of the 200 nm diameter suspended PS nanoparticles was likely due to a greater extent of confinement. The consistency in size-dependent aging rate of nanoparticles and thin films, when compared as a function of h^*, suggests a common cause of the aging confinement effect irrespective of confining geometry (*i.e.*, the free surface). A recent study by Roth and co-workers, who used ellipsometry to measure the physical aging rate of supported PS films, suggested a strong connection between the free surface (gradient in dynamics away from free surface) and aging confinement effects.[40]

Capping of the PS nanoparticles with a silica shell should remove the soft interface by confining the polymer within a hard shell, that is, the case of hard confinement. In addition, the rigid shell layer created an isochoric condition for structural relaxation. Since the shell layer was formed at room temperature, T_{room}, at $T_a > T_{room}$ a positive pressure, $\Delta P = \alpha_g \kappa_g (T_a - T_{room})$, would develop within the core−shell nanoparticles. In comparison to the corresponding aqueous suspended PS nanoparticles, silica-capped PS nanoparticles confined within a silica shell exhibited lower physical aging rates. This result is consistent with there being an internal pressure within the capped nanoparticles; that is, the relaxation rate should decrease with increasing pressure. Yet, the time required to reach equilibrium was smaller for capped PS nanoparticles. This is presumably due to the absence and presence of an initial aging plateau at short aging times (as predicted by the TNM model) for PS nanoparticles with and without a silica shell, respectively.

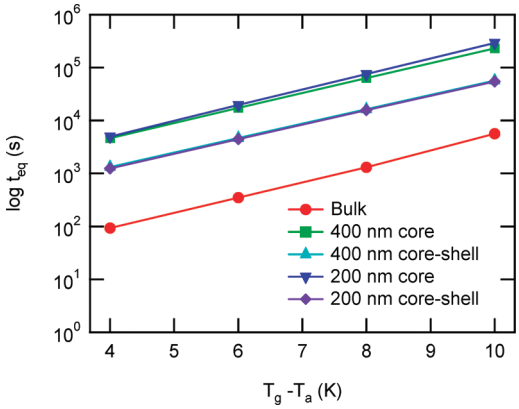

Figure 7. Time required for the attainment of equilibrium during aging for PS nanoparticles and bulk PS at different quench depths ($T_g - T_a$); t_{eq} is defined as the instant at which the value $T_f - T_a \leq 0.1$ K from the TNM model.

In an early report, Simon *et al.*[60] investigated the aging response of *ortho*-terphenyl (*o*-TP), a molecular glass former, under isochoric conditions. This was achieved by confining the *o*-TP in controlled pore glass. Interestingly, the isochorically confined *o*-TP aged to a nonzero value of $T_f - T_a$. That $T_f - T_a \neq 0$ at equilibrium was due to the formation of a negative pressure during vitrification. Thus, at all aging temperatures ($T_a < T_g$), *o*-TP aged under tension, which led to a modification of the apparent equilibrium state. In the current study, the state-of-affairs described above (*i.e.*, aging under tension) would not occur unless $T_a < T_{room}$, an aging condition not investigated in the current study.

CONCLUSIONS

In summary, we have investigated the glassy-state structural relaxation of PS nanoparticles under soft and hard confinement. Aqueous suspended PS and silica-capped PS nanoparticles aged under isobaric and isochoric conditions, respectively. We found that with decreasing diameter aqueous suspended PS nanoparticles (soft confinement) exhibited higher logarithmic physical aging rates in comparison to the bulk. Silica-capped PS nanoparticles aged at reduced rates compared to the corresponding aqueous suspended PS nanoparticles, in agreement with there being an internal positive pressure within the core−shell nanoparticles. The aging behavior could be well captured *via* the TNM model of structural recovery.

EXPERIMENTAL SECTION

Materials. Styrene was purchased from Acros Organics (99% extra pure, stabilized) and deinhibited by washing three times with a 2 M sodium hydroxide solution and three times with Milli-Q water. Washed styrene was distilled under reduced pressure before use. All other chemicals were used as received: sodium hydroxide (WTL La-borbedarf GmbH, 99%), divinylbenzene (Fluka, mixture of isomers ≈80%), ammonium persulfate (Acros Organics, 98%), acrylic acid (Acros Organics, 99.5%, stabilized), absolute ethanol (Sigma Aldrich), poly(allylamine

hydrochloride) (PAH, Aldrich, average $M_w \approx 15\,000$ g/mol), polyvinylpyrrolidone (PVP, Fluka, K 90, $M_w \approx 360\,000$ g/mol), ammonia (Fluka, 25 wt % in water), and tetraethoxysilane (TES, $Si(OEt)_4$) (Acros Organics, 98%). Milli-Q water was obtained from a Millipore purification system operating at 18.2 MΩ cm.

Synthesis of Polystyrene Nanoparticles. Soap-free emulsion polymerization was carried out in a 500 mL three-necked flask equipped with a condenser, a PTFE stirrer, and a gas inlet. Milli-Q water was put in the reactor, and nitrogen was bubbled for 20 min. Ammonium persulfate was added to the water, and the system was heated to 75 °C. A mixture of divinylbenzene, acrylic acid, and styrene was added dropwise within 1 h while stirring and reacted for 24 h. The resulting suspension was cleaned by centrifugation in water and ethanol at least six times. The resulting PS nanoparticles were suspended in water. The PS nanoparticles were slightly cross-linked with 0.4% and 1.3% w/w of divinylbenzene with respect to styrene for 200 and 400 nm PS nanoparticles, respectively.

Synthesis of Silica-Capped PS Nanoparticles. Polystyrene spheres were dispersed in water (concentration of 68 g/L) and pretreated with polyelectrolytes according to the procedure outlined in ref 61. Treated PS spheres were reacted with ammonia and TES at room temperature (23 °C) for 12 h while stirring, as previously described.[62] The spheres were washed three times in fresh ethanol. The resulting PS−silica nanoparticles were suspended in water.

SEM Imaging. PS nanoparticles and PS−silica core−shell nanoparticles were first dried in a fume hood at room temperature for 24 h then annealed at 50 °C in DSC pans until a stable heat flow was recorded. Dried samples were transferred onto black carbon tape and coated by sputtering with iridium for 20 min and then imaged using a Philips XL30 FEG SEM.

Calorimetry Measurements. Physical aging measurements were performed using a TA Instruments Q2000 differential scanning calorimeter (DSC) in both standard mode (for PS−silica core−shell nanoparticles and bulk PS) and modulated mode (MDSC) (for PS nanoparticles suspended in water). A nitrogen environment was employed in this study. The DSC was calibrated on heating at 20 °C/min and isothermally calibrated at 75 °C. The MDSC was calibrated on heating at 5 °C/min. Calibrations were performed using the modules in the Thermal Advantage software provided by TA Instruments.

Sample Preparation. PS nanoparticle (or PS−silica core−shell nanoparticle) suspensions were added dropwise into aluminum DSC pans held at 50 °C to partially evaporate water (core−shell nanoparticle samples were completely dried). After partial evaporation of water, another drop of the suspension was added to the pan and the water allowed to evaporate. This process was repeated twice to increase the mass of polymer in the sample pan. Samples were hermetically sealed, and as such, measurements were performed in an air (PS−silica core−shell nanoparticles) or water (PS nanoparticles) environment in the DSC pan. Bulk PS was prepared from nanoparticle samples that were dried under vacuum and subsequently annealed at 423 K for 20 h, which caused the particles to aggregate and form a bulk sample. SEM images (not shown) reveal the formation of bulk polymer by the above annealing protocol.

REFERENCES AND NOTES

1. Feng, W.; Patel, S. H.; Young, M. Y.; Zunino, J. L.; Xanthos, M. Smart Polymeric Coatings—Recent Advances. *Adv. Polym. Tech.* **2007**, *26*, 1–13.
2. Lin, Q. Properties of Photoresist Polymers. In *Physical Properties of Polymers Handbook*; Mark, J. E., Ed.; Springer: New York, 2007; p 965.
3. Mayer, A. C.; Scully, S. R.; Hardin, B. E.; Rowell, M. W.; McGehee, M. D. Polymer-Based Solar Cells. *Mater. Today* **2007**, *10*, 28–33.
4. Moniruzzaman, M.; Winey, K. I. Polymer Nanocomposites Containing Carbon Nanotubes. *Macromolecules* **2006**, *39*, 5194–5295.
5. Stern, S. A. Polymers for Gas Separations: The Next Decade. *J. Membr. Sci.* **1994**, *94*, 1–65.
6. de Gennes, P. G. Glass Transitions in Thin Polymer Films. *Eur. Phys. J. E* **2000**, *2*, 201–205.
7. Ellison, C. J.; Kim, S. D.; Hall, D. B.; Torkelson, J. M. Confinement and Processing Effects on Glass Transition Temperature and Physical Aging in Ultrathin Polymer Films: Novel Fluorescence Measurements. *Eur. Phys. J. E* **2002**, *8*, 155–166.
8. Ellison, C. J.; Torkelson, J. M. The Distribution of Glass-Transition Temperatures in Nanoscopically Confined Glass Formers. *Nat. Mater.* **2003**, *2*, 695–700.
9. Forrest, J. A.; Dalnoki-Veress, K. The Glass Transition in Thin Polymer Films. *Adv. Colloid Interface Sci.* **2001**, *94*, 167–196.
10. Forrest, J. A.; Dalnoki-Veress, K.; Stevens, J. R.; Dutcher, J. R. Effect of Free Surfaces on the Glass Transition Temperature of Thin Polymer Films. *Phys. Rev. Lett.* **1996**, *77*, 2002–2005.
11. Keddie, J. L.; Jones, R. A. L.; Cory, R. A. Size-Dependent Depression of the Glass Transition Temperature in Polymer Films. *Europhys. Lett.* **1994**, *27*, 59–64.
12. Keddie, J. L.; Jones, R. A. L.; Cory, R. A. Interface and Surface Effects on the Glass-Transition Temperature in Thin Polymer-Films. *Faraday Discuss.* **1994**, *98*, 219–230.
13. Mattsson, J.; Forrest, J. A.; Borjesson, L. Quantifying Glass Transition Behavior in Ultrathin Free-Standing Polymer Films. *Phys. Rev. E* **2000**, *62*, 5187–5200.
14. Park, C. H.; Kim, J. H.; Ree, M.; Sohn, B.; Jung, J. C.; Zin, W. Thickness and Composition Dependence of the Glass Transition Temperature in Thin Random Copolymer Films. *Polymer* **2004**, *45*, 4507–4513.
15. Priestley, R. D. Physical Aging of Confined Glasses. *Soft Matter* **2009**, *5*, 919–926.
16. Priestley, R. D.; Broadbelt, L. J.; Torkelson, J. M. Transition Glass and Alpha-Relaxation Dynamics of Thin Films of Labeled Polystyrene. *Phys. Rev. E* **2007**, *75*, 061806.
17. Priestley, R. D.; Ellison, C. J.; Broadbelt, L. J.; Torkelson, J. M. Structural Relaxation of Polymer Glasses at Surfaces, Interfaces and In Between. *Science* **2005**, *309*, 456–459.
18. Roth, C. B.; Dutcher, J. R. Glass Transition Temperature of Freely-Standing Films of Atactic Poly(methyl methacrylate). *Eur. Phys. J. E* **2003**, *12*, S103–S107.
19. Sharp, J. S.; Forrest, J. A. Free Surfaces Cause Reductions in the Glass Transition Temperature of Thin Polystyrene Films. *Phys. Rev. Lett.* **2003**, *91*, 23571.
20. Kranbuehl, D.; Knowles, R.; Hossain, A.; Hurt, M. Modeling the Effects of Confinement on the Glass Transition Temperature and Segmental Mobility. *J. Phys.: Condens. Matter.* **2003**, *15*, S1019–S1029.
21. Priestley, R. D.; Mundra, M. K.; Barnett, N. J.; Broadbelt, L. J.; Torkelson, J. M. Effects of Nanoscale Confinement and Interfaces on The Glass Transition Temperatures of a Series of Poly(*n*-methacrylate) Films. *Aust. J. Chem.* **2007**, *60*, 765–771.
22. Fakhraai, Z.; Sharp, J. S.; Forrest, J. A. Effect of Sample Preparation on the Glass-Transition of Thin Polystyrene Films. *J. Polym. Sci. B: Polym. Phys.* **2004**, *42*, 4503–4507.
23. Roth, C. B.; Dutcher, J. R. Glass Transition and Chain Mobility in Thin Polymer Films. *J. Electroanal. Chem.* **2005**, *584*, 13–22.
24. Alcoutlabi, M.; McKenna, G. B. Effects of Confinement on Materials Behavior at the Nanometre Size Scale. *J. Phys.: Condens. Matter.* **2005**, *17*, R461–R524.
25. Forrest, J. A.; Dalnoki-Veress, K.; Dutcher, J. R. Interface and Chain Confinement Effects on the Glass Transition Temperature of Thin Polymer Films. *Phys. Rev. E* **1997**, *56*, 5705–5716.
26. Fukao, K.; Miyamoto, Y. Glass Transitions and Dynamics in Thin Polymer Films: Dielectric Relaxation of Thin Films of Polystyrene. *Phys. Rev. E* **2000**, *61*, 1743–1754.
27. Papaleo, R. M.; Leal, R.; Carreira, W. H.; Barbosa, L. G.; Bello, I.; Bulla, A. Relaxation Times of Nanoscale Deformation on the Surface of a Polymer Thin Film near and below the Glass Transition. *Phys. Rev. B* **2006**, *74*, 094203.
28. Cheng, W.; Sainidou, R.; Burgardt, P.; Stefanou, N.; Kiyanova, A.; Efremov, M.; Fytas, G.; Nealey, P. F. Elastic Properties and Glass Transition of Supported Polymer Thin Films. *Macromolecules* **2007**, *40*, 7283–7290.
29. Lu, H.; Chen, W.; Russell, T. P. Relaxation of Thin Films of Polystyrene Floating on Ionic Liquid Surface. *Macromolecules* **2009**, *42*, 9111–9117.

30. Sasaki, T.; Shimizu, A.; Mourey, T. H.; Thurau, C. T.; Ediger, M. D. Glass Transition of Small Polystyrene Spheres in Aqueous Suspensions. *J. Chem. Phys.* **2003**, *119*, 8730–8735.
31. Serghei, A.; Huth, H.; Schellenberger, M.; Schick, C.; Kremer, F. Pattern Formation in Thin Polystyrene Films Induced by an Enhanced Mobility in Ambient Air. *Phys. Rev. E* **2005**, *71*, 061801.
32. Tress, M.; Erber, M.; Mapesa, E. U.; Huth, H.; Muller, J.; Serghei, A.; Schick, C.; Eichhorn, K.-J.; Voit, B.; Kremer, F. Glassy Dynamics and Glass Transition in Nanometric Thin Layers of Polystyrene. *Macromolecules* **2010**, *43*, 9937–9944.
33. van Zanten, J. H.; Wallace, W. E.; Wu, W. Effect of Strongly Favorable Substrate Interactions on the Thermal Properties of Ultrathin Polymer Films. *Phys. Rev. E* **1996**, *53*, R2053–R2056.
34. Dorkenoo, K.; Pfromm, P. H. Accelerated Physical Aging of Thin Poly[1-(trimethylsilyl)-1-propyne] Films. *Macromolecules* **2000**, *33*, 3747–3751.
35. Huang, Y.; Paul, D. R. Physical Aging of Thin Glassy Polymer Films Monitored by Gas Permeability. *Polymer* **2004**, *45*, 8377–8393.
36. Kawana, S.; Jones, R. A. L. Effect of Physical Ageing in Thin Glassy Polymer Films. *Eur. Phys. J. E* **2003**, *10*, 223–230.
37. Koh, Y. P.; Simon, S. L. Structural Relaxation of Stacked Ultrathin Polystyrene Films. *J. Polym. Sci. B: Polym. Phys.* **2008**, *46*, 2741–2753.
38. Priestley, R. D.; Broadbelt, L. J.; Torkelson, J. M. Physical Aging of Ultrathin Polymer Films Above and Below the Bulk Glass Transition Temperature: Effects of Attractive *vs* Neutral Polymer−Substrate Interactions Measured by Fluorescence. *Macromolecules* **2005**, *38*, 654–657.
39. Priestley, R. D.; Rittigstein, P.; Broadbelt, L. J.; Torkelson, J. M. Evidence for the Molecular-Scale Origin of the Suppression of Physical Aging in Confined Polymer: Fluorescence and Dielectric Studies of Polymer−Silica Nanocomposites. *J. Phys.: Condens. Matter.* **2007**, *19*, 205120.
40. Pye, J. E.; Rohald, K. A.; Baker, E. A.; Roth, C. B. Physical Aging in Ultrathin Polystyrene Films: Evidence of a Gradient in Dynamics at the Free Surface and Its Connection to the Glass Transition Temperature Reductions. *Macromolecules* **2010**, *43*, 8296–8303.
41. Rittigstein, P.; Priestley, R. D.; Broadbelt, L. J.; Torkelson, J. M. Model Polymer Nanocomposites Provides an Understanding of Confinement Effects in Real Nanocomposites. *Nat. Mater.* **2007**, *6*, 278–282.
42. Wu, J.; Huang, G.; Wang, X.; He, X.; Lei, H. Confinement Effect of Polystyrene on the Relaxation Behavior of Polyisobutylene. *J. Polym. Sci. B: Polym. Phys.* **2010**, *48*, 2165–2172.
43. Zhou, C.; Chung, T.; Wang, R.; Goh, S. H. A Governing Equation for Physical Aging of Thick and Thin Fluoropolyimide Films. *J. Appl. Polym. Sci.* **2004**, *92*, 1758–1764.
44. Rittigstein, P.; Torkelson, J. M. Polymer−Nanoparticle Interfacial Interactions in Polymer Nanocomposites: Confinement Effects on Glass Transition Temperature and Suppression of Physical Aging. *J. Polym. Sci. B: Polym. Phys.* **2006**, *44*, 2935–2943.
45. Liu, A. Y. H.; Rottler, J. Physical Aging and Structural Relaxation in Polymer Nanocomposites. *J. Polym. Sci. B: Polym. Phys.* **2009**, *47*, 1789–1798.
46. Mukherji, D.; Muser, M. H. Glassy Dynamics, Aging in Mobility, and Structural Relaxation of Strongly Adsorbed Polymer Films: Corrugation or Confinement?. *Macromolecules* **2007**, *40*, 1754–1762.
47. Debenedetti, P. G.; Stillinger, F. H. Supercooled Liquids and The Glass Transition. *Nature* **2001**, *410*, 259–267.
48. Zhang, C.; Guo, Y.; Priestley, R. D. The Glass Transition Temperature of Polymer Nanoparticles under Soft and Hard Confinement. *Macromolecules* **2011**, *44*, 4001–4006.
49. Debolt, M. A.; Easteal, A. J.; Macedo, P. B.; Moynihan, C. T. Analysis of Structural Relaxation in Glass Using Rate Heating Data. *J. Am. Ceram. Soc.* **1976**, *59*, 16–21.
50. Moynihan, C. T.; Easteal, A. J.; Debolt, M. A. Dependence of the Fictive Temperature of Glass on Cooling Rate. *J. Am. Ceram. Soc.* **1976**, *59*, 12–16.
51. Moynihan, C. T.; Macedo, P. B.; Montrose, C. J.; Gupta, P. K.; Debolt, M. A.; Dill, J. F.; Dom, B. E.; Drake, P. W.; Easteal, A. J.; Elterman, P. B.; *et al.* Structural Relaxation in Vitreous Materials. *Ann. N.Y. Acad. Sci.* **1976**, *279*, 15–35.
52. Narayanaswamy, O. S. Model of Structural Relaxation in Glass. *J. Am. Ceram. Soc.* **1971**, *54*, 491–497.
53. Tool, A. Q. Relation between Inelastic Deformability and Thermal Expansion of Glass in Its Annealing Range. *J. Am. Ceram. Soc.* **1946**, *29*, 240–253.
54. Kovacs, A. J.; Aklonis, J. J.; Hutchinson, J. M.; Ramos, A. R. Isobaric Volume and Enthalpy Recovery of Glasses: A Transparent Multiparameter Theory. *Macromolecules* **1979**, *17*, 1097–1162.
55. Kohlrausch, F. Ueber die Elastiche Nachwirkung Bei der Torsion. *Poogendorff's Annalen der Physik und Chemie* **1863**, *119*, 337–368.
56. Simon, S. L.; Sobieski, J. W.; Plazek, D. J. Volume and Enthalpy Recovery of Polystyrene. *Polymer* **2001**, *42*, 2555–2567.
57. Guo, Y.; Wang, N.; Bradshaw, R. D.; Brinson, L. C. Modeling Mechanical Aging Shift Factors in Glassy Polymers during Nonisothermal Physical Aging: Experiments and KAHR-ate Model Prediction. *J. Polym. Sci. B: Polym. Phys.* **2009**, *47*, 340.
58. Badrinarayanan, P.; Zheng, W.; Li, Q.; Simon, S. L. The Glass Transition *versus* the Fictive Temperature. *J. Non-Cryst. Solids* **2007**, *353*, 2603–2612.
59. Greiner, R.; Schwarzl, F. R. Thermal Contraction and Volume Relaxation of Amorphous Polymers. *Rheol. Acta* **1984**, *23*, 378–395.
60. Simon, S. L.; Park, J. Y.; McKenna, G. B. Enthalpy Recovery of a Glass-Forming Liquid Constrained in a Nanoporous Matrix: Negative Pressure Effects. *Eur. Phys. J. E* **2002**, *8*, 209–216.
61. Graf, C.; Vossen, D. L. J.; Imhof, A.; van Blaaderen, A. A General Method To Coat Colloidal Particles with Silica. *Langmuir* **2003**, *19*, 6693–6700.
62. Zhang, L.; D'Acunzi, M.; Kappl, M.; Auernhammer, G. K.; Vollmer, D. Hollow Silica Spheres: Synthesis and Mechanical Properties. *Langmuir* **2009**, *25*, 2711–2717.